Mon. Not. R. Astron. Soc. **363,** 268–284 (2005) doi:10.1111/j.1365-2966.2005.09436.x

Relativistic models of galaxies

D. Vogt[1]★ and P. S. Letelier[2]★†

[1]*Instituto de Física Gleb Wataghin, Universidade Estadual de Campinas 13083-970 Campinas, S. P., Brazil*
[2]*Departamento de Matemática Aplicada-IMECC, Universidade Estadual de Campinas 13083-970 Campinas, S. P., Brazil*

Accepted 2005 July 18. Received 2005 July 14; in original form 2005 March 23

ABSTRACT

A special form of the isotropic metric in cylindrical coordinates is used to construct what may be interpreted as the general relativistic versions of some well-known potential–density pairs used in Newtonian gravity to model three-dimensional distributions of matter in galaxies. The components of the energy-momentum tensor are calculated for the first two Miyamoto–Nagai potentials and a particular potential due to Satoh. The three potentials yield distributions of matter in which all tensions are pressures and all energy conditions are satisfied for certain ranges of the free parameters. A few non-planar geodesic orbits are computed for one of the potentials and compared with the Newtonian case. Rotation is also incorporated in the models and the effects of the source rotation on the rotation profile are calculated as first-order corrections by using an approximate form of the Kerr metric in isotropic coordinates.

Key words: relativity – stellar dynamics – celestial mechanics – galaxies: kinematics and dynamics.

1 INTRODUCTION

Analytical axially symmetric solutions of gravitating matter provide very accurate models for the mass distribution of galaxies. In Newtonian theory, models for globular clusters and spherical galaxies were presented by Plummer (1911) and King (1966). On the other hand, to describe the mass distribution within highly flattened axisymmetric galaxies, Toomre (1963) found a family of density potential pairs, the first of which was first derived by Kuzmin (1956). Later, Miyamoto & Nagai (1975) and Nagai & Miyamoto (1976) 'thickened-up' Toomre's series of disc models to yield pairs of three-dimensional potential and density functions. In a similar way, Satoh (1980) obtained a family of three-dimensional axisymmetric mass distributions from the higher-order Plummer models. For a detailed account and the description of other potential–density pairs used in galactic models, see for example Binney & Tremaine (1987).

In general relativity, several exact disc-like solutions have been found, among them the static discs without radial pressure studied by Bonnor & Sackfield (1968) and Morgan & Morgan (1969), and discs with radial pressure by Morgan & Morgan (1970). Several classes of exact solutions of the Einstein field equations corresponding to static thin discs with or without radial pressure have been obtained by different authors (Lynden-Bell & Pineault 1978; Letelier & Oliveira 1987; Lemos 1989; Bičák, Lynden-Bell & Katz 1993a; Bičák, Lynden-Bell & Pichon 1993b; Lemos & Letelier 1993, 1994, 1996; González & Espitia 2003; García & González 2004). Thin rotating discs that can be considered as a source of the Kerr metric were presented by Bičák & Ledvinka (1993), while rotating discs with heat flow were studied by González & Letelier (2000). Also thin discs with radial tension (González & Letelier 1999), magnetic fields (Letelier 1999) and magnetic and electric fields (Katz, Bičák & Lynden-Bell 1999) were considered. The non-linear superposition of a disc and a black hole was first obtained by Lemos & Letelier (1993). Perfect fluid discs with haloes were studied by Vogt & Letelier (2003) and charged perfect fluid discs by Vogt & Letelier (2004). The stability of some general relativistic thin disc models using a first-order perturbation of the energy-momentum tensor was investigated by Ujevic & Letelier (2004). For a survey on self-gravitating relativistic discs, see for instance Karas, Huré & Semerák (2004).

In the works cited above, an inverse style method was used to solve the Einstein equations, i.e. the energy-momentum tensor is computed from the metric representing the disc. Another approach to generate discs is by solving the Einstein equations given a source (energy-momentum tensor). Essentially, they are obtained by solving a Riemann–Hilbert problem and are highly non-trivial. This has been used by the Jena group to generate several exact solutions of discs (Neugebauer & Meinel 1995; Klein 1997, 2001, 2002, 2003a,b; Klein & Richter 1999; Frauendiener & Klein 2001).

★E-mail: danielvt@ifi.unicamp.br (DV); letelier@ime.unicamp.br (PSL)
†URL: http://www.ime.unicamp.br/∼letelier/

Recently, González & Letelier (2004) constructed models of static relativistic thick discs in various coordinate systems. Although the discs have constant thickness, the matter density decreases rapidly with radius and the z coordinate, and in principle they may also be used to represent both the disc part and the central bulges of galaxies.

The aim of this work is to consider more realistic three-dimensional models for the gravitational field of galaxies in a general relativistic context. The distribution of matter fills all the space, but the total mass is finite. Essentially we formulate general relativistic versions in isotropic coordinates of the potential–density pairs deduced by Miyamoto & Nagai (1975), Nagai & Miyamoto (1976) and Satoh (1980). Also, the influence of galactic rotation on the rotation profile of test particles on the galactic plane is estimated using an approximate form of the Kerr metric in isotropic coordinates.

The paper is organized as follows. In Section 2 we present a special form of the isotropic metric and the components of the energy-momentum tensor as functions of the metric coefficients, from which the physical properties of the galactic matter distributions can be calculated. We also derive expressions for the tangential circular velocity and specific angular momentum of test particles in circular motion on the galactic plane. These results are then applied in Sections 3 and 4 to construct general relativistic analogues of two Miyamoto–Nagai models and one galactic model proposed by Satoh. As an example of application of these models, in Section 5 we calculate a few geodesic orbits and compare them with the Newtonian case. In Section 6 we deduce the first-order effects of galactic rotation on the tangential circular velocity of geodesic motion of particles on the galactic plane using an approximate form of the Kerr metric in isotropic coordinates, and we apply the result to the above-mentioned models. Finally, we summarize our results in Section 7.

2 EINSTEIN EQUATIONS IN ISOTROPIC COORDINATES

Let us consider the particular case of axial symmetric space–times whose metric can be written in an isotropic form in cylindrical coordinates (t, R, z, φ),

$$\mathrm{d}s^2 = \mathrm{e}^{\nu(R,z)}c^2\mathrm{d}t^2 - \mathrm{e}^{\lambda(R,z)}\left(\mathrm{d}R^2 + \mathrm{d}z^2 + R^2\mathrm{d}\varphi^2\right). \tag{1}$$

In order to construct a general relativistic formulation of the known Newtonian models for the mass distribution of galaxies, it is convenient to use a particular form of metric equation (1), suggested by generalizing the form of the Schwarzschild metric in isotropic coordinates

$$\mathrm{d}s^2 = \left(\frac{1-f}{1+f}\right)^2 c^2\mathrm{d}t^2 - (1+f)^4(\mathrm{d}R^2 + \mathrm{d}z^2 + R^2\mathrm{d}\varphi^2), \tag{2}$$

where $f = f(R, z)$. Metric equation (2) gives the Schwarzschild solution when f is taken as

$$f = \frac{GM}{2c^2\sqrt{R^2+z^2}}. \tag{3}$$

For metric equation (2), the Einstein equations $G_{\mu\nu} = -(8\,\pi G/c^4)\,T_{\mu\nu}$ yield the following expressions for the components of the energy-momentum tensor:[1]

$$T_t^t = -\frac{c^4}{2\pi G(1+f)^5}\left(f_{,RR} + f_{,zz} + \frac{f_{,R}}{R}\right), \tag{4a}$$

$$T_R^R = \frac{c^4}{4\pi G(1+f)^5(1-f)}\left(ff_{,zz} + \frac{ff_{,R}}{R} + 2f_{,R}^2 - f_{,z}^2\right), \tag{4b}$$

$$T_z^z = \frac{c^4}{4\pi G(1+f)^5(1-f)}\left(ff_{,RR} + \frac{ff_{,R}}{R} + 2f_{,z}^2 - f_{,R}^2\right), \tag{4c}$$

$$T_z^R = T_R^z = -\frac{c^4}{4\pi G(1+f)^5(1-f)}(ff_{,Rz} - 3f_{,R}f_{,z}), \tag{4d}$$

$$T_\varphi^\varphi = \frac{c^4}{4\pi G(1+f)^5(1-f)}\left[f(f_{,RR} + f_{,zz}) - f_{,R}^2 - f_{,z}^2\right]. \tag{4e}$$

The energy density is given by $\sigma = T_t^t/c^2$, and the stresses (pressures or tensions) along a particular direction read $P_i = -T_i^i$ when the energy-momentum tensor is diagonal. It is a surprising fact that the component T_t^t is proportional to the usual Laplacian of the function f in flat cylindrical coordinates. Note that in the Newtonian limit when $f \ll 1$, equation (4a) reduces to the Poisson equation

$$\nabla^2\Phi = 4\pi G\rho_N, \tag{5}$$

if the function f is related to the gravitational potential Φ by

$$f = -\frac{\Phi}{2c^2}. \tag{6}$$

[1] The Einstein tensor was computed using MAPLE and the result was checked using REDUCE.

The energy-momentum tensor will be diagonal ($T_z^R = T_R^z = 0$) provided f has the form

$$f = \frac{C}{\sqrt{w(R) + g(z)}}, \tag{7}$$

where C is a constant and $w(R)$ and $g(z)$ are arbitrary functions. Furthermore, the components T_R^R and T_φ^φ will be equal (isotropic radial and azimuthal stresses) only if $w(R) = R^2$.

Two physical quantities of interest related to the circular motion of test particles along geodesics on the galactic plane are the tangential velocity v_c (rotation profile) and the specific angular momentum h. The assumption of geodesic motion is valid for the case of a particle moving in a very diluted gas like the gas made of stars that models a galaxy disc. For metric equation (1) the expressions are (Vogt & Letelier 2003)

$$v_c^2 = c^2 R^2 \frac{\mathrm{e}^\lambda (\mathrm{e}^\nu)_{,R}}{\mathrm{e}^\nu (R^2 \mathrm{e}^\lambda)_{,R}}, \tag{8}$$

$$h = cR^2 \mathrm{e}^\lambda \sqrt{\frac{(\mathrm{e}^\nu)_{,R}}{\mathrm{e}^\nu (R^2 \mathrm{e}^\lambda)_{,R} - R^2 \mathrm{e}^\lambda (\mathrm{e}^\nu)_{,R}}}, \tag{9}$$

where all functions are evaluated on $z = 0$. The angular momentum can be used to determine the stability of circular orbits on the galactic plane by using an extension of the Rayleigh criteria of stability of a fluid at rest in a gravitational field (Rayleigh 1917; see also Landau & Lifshitz 1987)

$$h \frac{\mathrm{d}h}{\mathrm{d}R}\bigg|_{z=0} > 0. \tag{10}$$

For the specific metric form equation (2), equations (8) and (9) simplify to

$$v_c^2 = -\frac{2c^2 R f_{,R}}{(1-f)(1+f+2Rf_{,R})}, \tag{11}$$

$$h = cR^2 (1+f)^2 \sqrt{\frac{-2f_{,R}}{R\left[1 - f^2 + 2Rf_{,R}(2-f)\right]}}. \tag{12}$$

3 GENERAL RELATIVISTIC MIYAMOTO–NAGAI MODELS

3.1 First model

The simplest gravitational potential proposed by Miyamoto & Nagai (1975) and Nagai & Miyamoto (1976) to represent stratifications of mass in the central bulges and in the disc parts of galaxies is given by

$$\Phi(R, z) = -\frac{GM}{\sqrt{R^2 + (a + \sqrt{z^2 + b^2})^2}}, \tag{13}$$

where a and b are positive constants. The corresponding three-dimensional density distribution $\rho_N(R, z)$ is easily derived from Poisson equation (5)

$$\rho_N(R, z) = \frac{b^2 M}{4\pi} \frac{aR^2 + (a + 3\sqrt{z^2 + b^2})(a + \sqrt{z^2 + b^2})^2}{[R^2 + (a + \sqrt{z^2 + b^2})^2]^{5/2} (z^2 + b^2)^{3/2}}. \tag{14}$$

Now we consider the function $f(R, z)$ defined in the previous section as

$$f(R, z) = \frac{GM}{2c^2 \sqrt{R^2 + (a + \sqrt{z^2 + b^2})^2}}. \tag{15}$$

Substituting equation (15) in equations (4a)–(4e) we find the following expressions for the non-zero components of the energy-momentum tensor

$$\bar{\sigma} = \frac{\tilde{b}^2 [\tilde{a}\tilde{R}^2 + (\tilde{a} + \xi)^2 (\tilde{a} + 3\xi)]}{4\pi\xi^3 \left[1 + \sqrt{\tilde{R}^2 + (\tilde{a} + \xi)^2}\right]^5}, \tag{16a}$$

$$\bar{p}_R = \bar{p}_\varphi = \frac{\tilde{b}^2}{8\pi\xi^3} \frac{\left[\tilde{a}\tilde{R}^2 + (\tilde{a} + \xi)^2 (\tilde{a} + 2\xi)\right]}{\left[1 + \sqrt{\tilde{R}^2 + (\tilde{a} + \xi)^2}\right]^5 \left[-1 + \sqrt{\tilde{R}^2 + (\tilde{a} + \xi)^2}\right]}, \tag{16b}$$

$$\bar{p}_z = \frac{\tilde{b}^2 (\tilde{a} + \xi)^2}{4\pi\xi^2 \left[1 + \sqrt{\tilde{R}^2 + (\tilde{a} + \xi)^2}\right]^5 \left[-1 + \sqrt{\tilde{R}^2 + (\tilde{a} + \xi)^2}\right]}, \tag{16c}$$

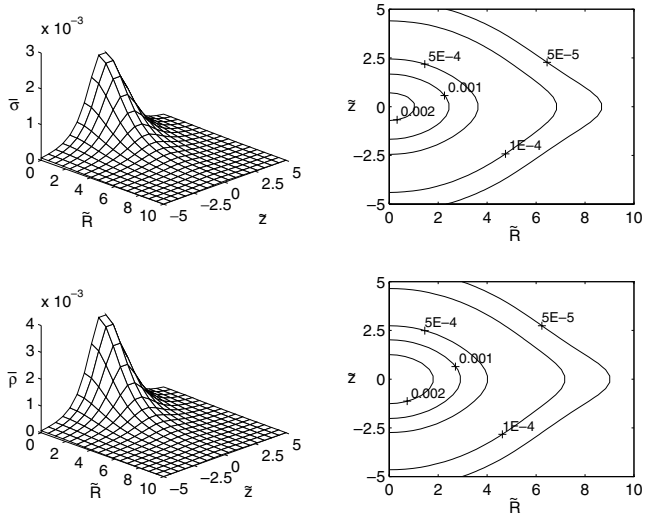

Figure 1. Surface plot and level curves of the energy density $\bar{\sigma}$ equation (16a) and 'effective Newtonian density' $\bar{\rho}$ equation (17) with parameters $\tilde{a} = 1$ and $\tilde{b} = 2$.

where the variables and parameters were rescaled in terms of the Schwarzschild radius in isotropic spherical coordinates $r_s = GM/(2c^2)$:[2] $\tilde{R} = R/r_s, \tilde{z} = z/r_s, \tilde{a} = a/r_s, \tilde{b} = b/r_s, \sigma = (M/r_s^3)\bar{\sigma}$, $p_i = (Mc^2/r_s^3)\bar{p}_i$ and $\xi = \sqrt{\tilde{z}^2 + \tilde{b}^2}$. The 'effective Newtonian density' $\rho = \sigma + p_R/c^2 + p_\varphi/c^2 + p_z/c^2$ reads

$$\bar{\rho} = \frac{\tilde{b}^2\sqrt{\tilde{R}^2 + (\tilde{a}+\xi)^2}\left[\tilde{a}\tilde{R}^2 + (\tilde{a}+\xi)^2(\tilde{a}+3\xi)\right]}{4\pi\xi^3\left[1+\sqrt{\tilde{R}^2+(\tilde{a}+\xi)^2}\right]^5\left[-1+\sqrt{\tilde{R}^2+(\tilde{a}+\xi)^2}\right]}, \tag{17}$$

with $\rho = (M/r_s^3)\bar{\rho}$.

The strong energy condition requires that $\rho \geqslant 0$, whereas the weak energy condition imposes the condition $\sigma \geqslant 0$. The dominant energy condition requires $|p_R/\sigma| \leqslant c^2$, $|p_z/\sigma| \leqslant c^2$ and $|p_\varphi/\sigma| \leqslant c^2$. Equations (16a)–(17) show that the densities are positive everywhere and so are the stresses (pressures) if we impose the condition $\tilde{a} + \tilde{b} > 1$. Moreover, we have isotropic pressures along the radial and azimuthal directions. When $\tilde{R}, \tilde{z}, \tilde{a}, \tilde{b} \gg 1$, the first-order expansion of equation (17) is

$$\bar{\rho} \approx \frac{\tilde{b}^2\left[\tilde{a}\tilde{R}^2 + (\tilde{a}+\xi)^2(\tilde{a}+3\xi)\right]}{4\pi\xi^3\left[\tilde{R}^2+(\tilde{a}+\xi)^2\right]^{5/2}}\left[1 - \frac{4}{\sqrt{\tilde{R}^2+(\tilde{a}+\xi)^2}}\right]. \tag{18}$$

Thus, the first-order general relativistic correction lowers the mass density.

In Figs 1 and 2 we show the surfaces and level curves of the densities and pressures equations (16a)–(17) for parameters $\tilde{a} = 1$ and $\tilde{b} = 2$, and the same physical quantities for parameters $\tilde{a} = 1$ and $\tilde{b} = 1$ are displayed in Figs 3 and 4. As in the Newtonian case, the lower the ratio b/a, the flatter the mass distributions, and the pressure distributions show similar behaviour. For $\tilde{a} = 1$ and $\tilde{b} = 2$ we have $\tilde{p}_R/\tilde{\sigma} < 0.2$ and $\tilde{p}_z/\tilde{\sigma} < 0.15$, and for $\tilde{a} = 1$ and $\tilde{b} = 1$ the ratios are $\tilde{p}_R/\tilde{\sigma} < 0.4$ and $\tilde{p}_z/\tilde{\sigma} < 0.3$. Thus, for these parameters all energy conditions are satisfied.

The tangential circular velocity equation (11) and specific angular momentum equation (12) for f given by equation (15) evaluated on $z = 0$ read

$$\left(\frac{v_c}{c}\right)^2 = \frac{2\tilde{R}^2\sqrt{\tilde{R}^2+\eta^2}}{\left(-1+\sqrt{\tilde{R}^2+\eta^2}\right)\left[-\tilde{R}^2+\eta^2+(\tilde{R}^2+\eta^2)^{3/2}\right]}, \tag{19}$$

$$\bar{h} = \frac{\sqrt{2}\tilde{R}^2\left(1+\sqrt{\tilde{R}^2+\eta^2}\right)^2}{(\tilde{R}^2+\eta^2)^{3/4}\sqrt{(\tilde{R}^2+\eta^2)^2+\tilde{R}^2-\eta^2-4\tilde{R}^2\sqrt{\tilde{R}^2+\eta^2}}}, \tag{20}$$

where we have defined $h = cr_s\bar{h}$ and $\eta = \tilde{a} + \tilde{b}$. The first-order expansion of equation (19) reads

$$\frac{v_c}{c} = \frac{\tilde{R}\sqrt{2}}{\left[\tilde{R}^2+(\tilde{a}+\tilde{b})^2\right]^{3/4}}\left\{1 + \frac{\tilde{R}^2}{\left[\tilde{R}^2+(\tilde{a}+\tilde{b})^2\right]^{3/2}}\right\}. \tag{21}$$

[2] Note that the Schwarzschild radius r_s in isotropic spherical coordinates is related to Schwarzschild radius r_s' in canonical spherical coordinates by $r_s = r_s'/4$.

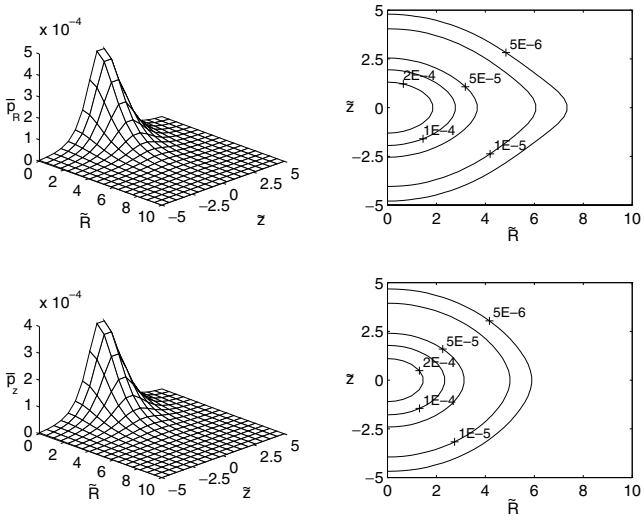

Figure 2. Surface plot and level curves of the radial pressure $\bar{p}_R$ equation (16a) and vertical pressure $\bar{p}_z$ equation (17) with parameters $\tilde{a} = 1$ and $\tilde{b} = 2$.

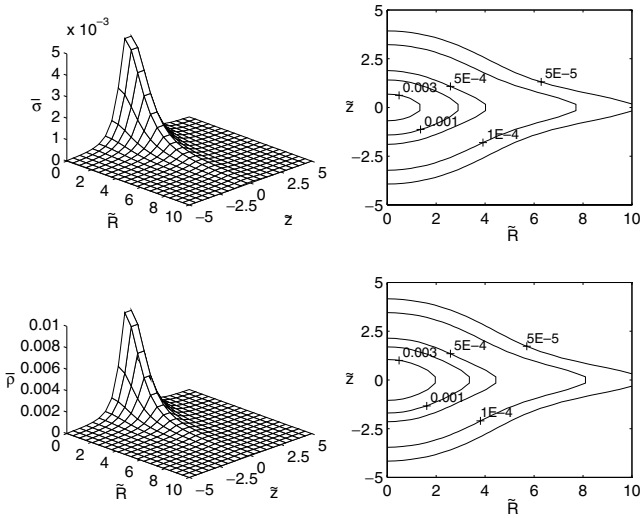

Figure 3. Surface plot and level curves of the energy density $\bar{\sigma}$ equation (16a) and 'effective Newtonian density' $\bar{\rho}$ equation (17) with parameters $\tilde{a} = 1$ and $\tilde{b} = 1$.

Figs 5(a) and (b) show, respectively, the rotation profile equation (19) and the curves of specific angular momentum equation (20) for parameters $\tilde{a} = 1$ and $\tilde{b} = 2$, $\tilde{b} = 1$ and $\tilde{b} = 0.5$. In Fig. 5(a) the dashed curves represent the Newtonian tangential velocities. Relativistic tangential velocities are always higher than the Newtonian ones, as suggested by the first-order correction in equation (21). The curves of specific angular momentum show that circular orbits on the plane $\tilde{z} = 0$ turn out to be unstable for higher flattened matter distributions (the curve for $\tilde{b} = 0.5$). The orbits for the parameters $\tilde{a} = 1$ and $\tilde{b} = 2$ are all stable, whereas in the case of $\tilde{b} = 1$ a small region of instability appears between $\tilde{R} \approx 5$ and $\tilde{R} \approx 6$. The Newtonian limit of equation (20) gives

$$\bar{h} = \frac{\sqrt{2}\tilde{R}^2}{[\tilde{R}^2 + (\tilde{a} + \tilde{b})^2]^{3/4}}, \tag{22}$$

from which it is easily checked that $(\mathrm{d}\bar{h}/\mathrm{d}\tilde{R}) \geqslant 0$ for all $\tilde{a}$, $\tilde{b}$ and $\tilde{R}$. Thus, the instability is a pure relativistic effect (the same is verified for circular orbits around the superposition of black holes and axially symmetric structures in Weyl coordinates; see Letelier 2003).

3.2 Second model

Another pair of potential and density functions presented by Miyamoto and Nagai as a generalization of the Toomre model 2 is described by

$$\Phi(R, z) = -\frac{GM}{\sqrt{R^2 + (a + \zeta)^2}} \left[1 + \frac{a(a + \zeta)}{R^2 + (a + \zeta)^2}\right], \tag{23a}$$

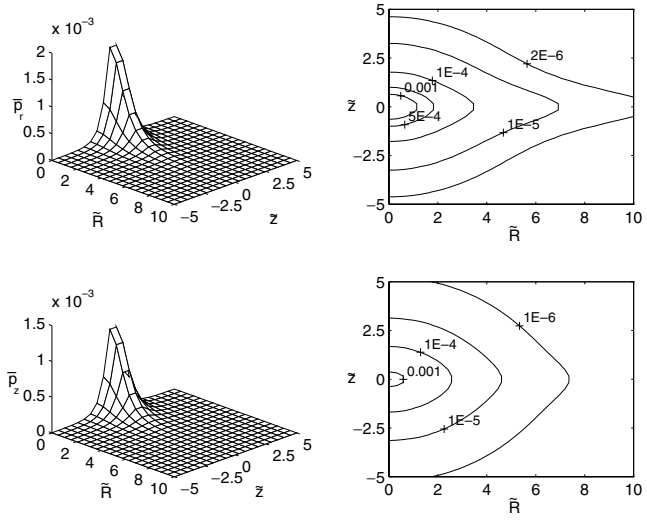

Figure 4. Surface plot and level curves of the radial pressure $\bar{p}_R$ equation (16b) and vertical pressure $\bar{p}_z$ equation (16c) with parameters $\tilde{a} = 1$ and $\tilde{b} = 1$.

$$\rho_N(R,z) = \frac{3b^2M}{4\pi\zeta^3[R^2+(a+\zeta)^2]^{7/2}}[R^2(a^3+\zeta^3)+(\zeta+a)^3(\zeta^2+4a\zeta+a^2)], \tag{23b}$$

where $\zeta = \sqrt{z^2+b^2}$. Using f defined by equation (6) in equations (4a)–(4e), we find that the components $T^R_z = T^z_R$ are non-zero. The physical variables of the matter distribution are obtained by solving the eigenvalue problem for T^a_b

$$T^a_b\,\Xi^b = \lambda\,\Xi^a. \tag{24}$$

We find that T^{ab} can be put in the form

$$T^{ab} = \sigma e^a_{(0)}e^b_{(0)} + p_+e^a_{(1)}e^b_{(1)} + p_-e^a_{(2)}e^b_{(2)} + p_\varphi e^a_{(3)}e^b_{(3)}, \tag{25}$$

where

$$\begin{aligned} \sigma &= \frac{T^t_t}{c^2}, \qquad e^a_{(0)} = \left(\frac{1+f}{1-f},0,0,0\right), \\ p_\pm &= -\frac{T^R_R+T^z_z}{2} \mp \frac{1}{2}\sqrt{(T^R_R-T^z_z)^2+4(T^R_z)^2}, \end{aligned} \tag{26}$$

$$\begin{aligned} e^a_{(1)} &= (0,e^R_{(1)},e^z_{(1)},0), \qquad e^a_{(2)} = (0,e^R_{(2)},e^z_{(2)},0), \\ p_\varphi &= -T^\varphi_\varphi, \qquad e^a_{(3)} = \left(0,0,0,\frac{1}{R(1+f)^2}\right), \end{aligned} \tag{27}$$

and

$$\begin{aligned} e^R_{(1)} &= -\frac{T^R_z}{(1+f)^2\sqrt{\left(T^R_z\right)^2+\left(T^R_R+p_+\right)^2}}, \qquad e^z_{(1)} = \frac{T^R_R+p_+}{(1+f)^2\sqrt{\left(T^R_z\right)^2+\left(T^R_R+p_+\right)^2}}, \\ e^R_{(2)} &= -\frac{T^R_z}{(1+f)^2\sqrt{\left(T^R_z\right)^2+\left(T^R_R+p_-\right)^2}}, \qquad e^z_{(2)} = \frac{T^R_R+p_-}{(1+f)^2\sqrt{\left(T^R_z\right)^2+\left(T^R_R+p_-\right)^2}}. \end{aligned} \tag{28}$$

The effective Newtonian density reads $\rho = \sigma + p_+/c^2 + p_-/c^2 + p_\varphi/c^2 = \sigma - T^R_R/c^2 - T^z_z/c^2 + p_\varphi/c^2$. The explicit expressions for $\bar{\sigma}$, $\bar{\rho}$ and $\bar{p}_\varphi$ are

$$\bar{\sigma} = \frac{3\tilde{b}^2\chi^4\left[\tilde{R}^2(\tilde{a}^3+\xi^3)+(\tilde{a}+\xi)^3(\tilde{a}^2+\xi^2+4\tilde{a}\xi)\right]}{4\pi\xi^3\left[\chi^{3/2}+\tilde{R}^2+(\tilde{a}+\xi)(2\tilde{a}+\xi)\right]^5}, \tag{29}$$

$$\bar{\rho} = \frac{3\tilde{b}^2\chi^{11/2}\left[\tilde{R}^2(\tilde{a}^3+\xi^3)+(\tilde{a}+\xi)^3(\tilde{a}^2+\xi^2+4\tilde{a}\xi)\right]}{4\pi\xi^3\left[\chi^{3/2}+\tilde{R}^2+(\tilde{a}+\xi)(2\tilde{a}+\xi)\right]^5\left[\chi^{3/2}-\tilde{R}^2-(\tilde{a}+\xi)(2\tilde{a}+\xi)\right]}, \tag{30}$$

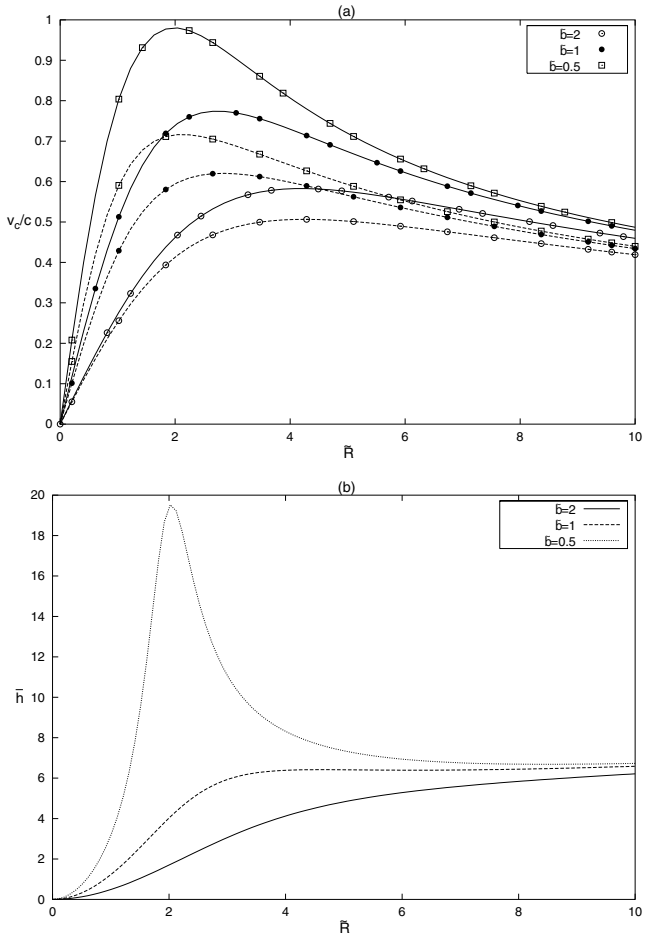

Figure 5. (a) Relativistic rotation profile equation (19) and Newtonian rotation profile (dashed curves) with parameters $\tilde{a} = 1$, $\tilde{b} = 2$, $\tilde{b} = 1$ and $\tilde{b} = 0.5$. (b) Specific angular momentum equation (20) for the same parameters.

$$\bar{p}_\varphi = \frac{\chi^4}{8\pi\xi^3\left[\chi^{3/2}+\tilde{R}^2+(\tilde{a}+\xi)(2\tilde{a}+\xi)\right]^5\left[\chi^{3/2}-\tilde{R}^2-(\tilde{a}+\xi)(2\tilde{a}+\xi)\right]}\left\{\tilde{R}^4\left[\xi^3(\tilde{a}^2+2\tilde{b}^2)+3\tilde{a}^3\tilde{b}^2\right]+\tilde{R}^2(\tilde{a}+\xi)^2\right.$$
$$\left.\times\left[9\tilde{a}^3\tilde{b}^2+12\tilde{a}\tilde{b}^2\xi^2+4\tilde{b}^2\xi^3+2\tilde{a}^2(7\tilde{b}^2+\tilde{z}^2)\xi\right]+(a+\xi)^4\left[6\tilde{a}^3\tilde{b}^2+12\tilde{a}\tilde{b}^2\xi^2+2\tilde{b}^2\xi^3+\tilde{a}^2(19\tilde{b}^2+\tilde{z}^2)\xi\right]\right\}, \tag{31}$$

where $\xi = \sqrt{\tilde{z}^2+\tilde{b}^2}$, $\chi = \tilde{R}^2+(\tilde{a}+\xi)^2$ and the dimensionless variables were previously defined. The components T_R^R, T_z^R and T_z^z read

$$T_R^R = -\frac{Mc^2}{r_s^3}\frac{\chi^4}{8\pi\xi^3\left[\chi^{3/2}+\tilde{r}^2+(\tilde{a}+\xi)(2\tilde{a}+\xi)\right]^5\left[\chi^{3/2}-\tilde{r}^2-(\tilde{a}+\xi)(2\tilde{a}+\xi)\right]}\left\{\tilde{r}^4\left[\xi^3(\tilde{a}^2+2\tilde{b}^2)+3\tilde{a}^3\tilde{b}^2\right]+\tilde{r}^2(\tilde{a}+\xi)^2\right.$$
$$\left.\times\left[9\tilde{a}^3\tilde{b}^2+12\tilde{a}\tilde{b}^2\xi^2+4\tilde{b}^2\xi^3+2\tilde{a}^2(\tilde{b}^2-5\tilde{z}^2)\xi\right]+(\tilde{a}+\xi)^4\left[6\tilde{a}^3\tilde{b}^2+12\tilde{a}\tilde{b}^2\xi^2+2\tilde{b}^2\xi^3+\tilde{a}^2(19\tilde{b}^2+\tilde{z}^2)\xi\right]\right\}, \tag{32}$$

$$T_z^R = T_R^z = -\frac{Mc^2}{r_s^3}\frac{3\tilde{a}^2\tilde{r}\tilde{z}(\tilde{a}+\xi)\chi^4\left[\tilde{r}^2-(a+\xi)^2\right]}{4\pi\xi\left[\chi^{3/2}+\tilde{r}^2+(\tilde{a}+\xi)(2\tilde{a}+\xi)\right]^5\left[\chi^{3/2}-\tilde{r}^2-(\tilde{a}+\xi)(2\tilde{a}+\xi)\right]}, \tag{33}$$

$$T_z^z = \frac{Mc^2}{r_s^3}\frac{\chi^4}{4\pi\xi^2\left[\chi^{3/2}+\tilde{r}^2+(\tilde{a}+\xi)(2\tilde{a}+\xi)\right]^5\left[\chi^{3/2}-\tilde{r}^2-(\tilde{a}+\xi)(2\tilde{a}+\xi)\right]}$$
$$\times\left\{\tilde{r}^4\xi^2(\tilde{a}^2-\tilde{b}^2)-2\tilde{r}^2\xi(\tilde{a}+\xi)^2\left[3\tilde{a}\tilde{b}^2+\xi(2\tilde{a}^2+\tilde{b}^2)\right]+(\tilde{a}+\xi)^4\left[\tilde{a}^2(\tilde{z}^2-8\tilde{b}^2)-\tilde{b}^2\xi(6\tilde{a}+\xi)\right]\right\}, \tag{34}$$

and $p_\pm$ is further adimensionalized as $p_\pm = (Mc^2/r_s^3)\bar{p}_\pm$.

The condition $(\tilde{a}+\tilde{b})^2 > (2\tilde{a}+\tilde{b})$ ensures positive densities and non-singular behaviour for the densities and pressures. The first-order expansion of equation (30) reads

$$\bar{\rho} \approx \frac{3\tilde{b}^2\left[\tilde{R}^2(\tilde{a}^3+\xi^3)+(\tilde{a}+\xi)^3(\tilde{a}^2+\xi^2+4\tilde{a}\xi)\right]}{4\pi\xi^3[\tilde{R}^2+(\tilde{a}+\xi)^2]^{7/2}}\left\{1-\frac{4[\tilde{R}^2+(\tilde{a}+\xi)(2\tilde{a}+\xi)]}{[\tilde{R}^2+(\tilde{a}+\xi)^2]^{3/2}}\right\}. \tag{35}$$

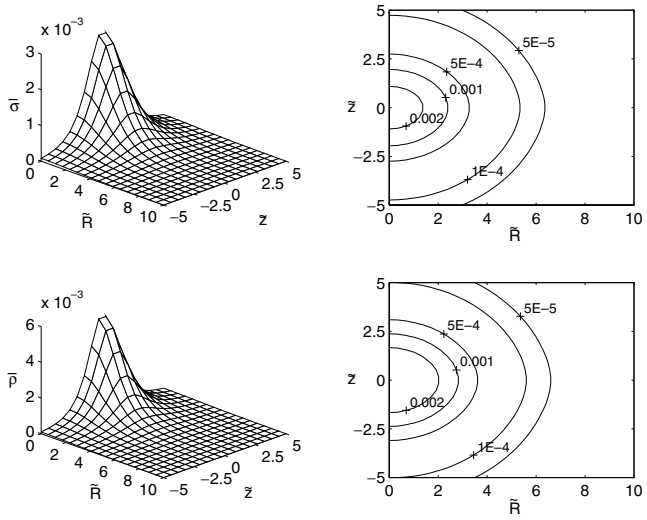

Figure 6. Surface plot and level curves of the energy density $\bar{\sigma}$ equation (29) and 'effective Newtonian density' $\bar{\rho}$ equation (30) with parameters $\tilde{a} = 1$ and $\tilde{b} = 2$.

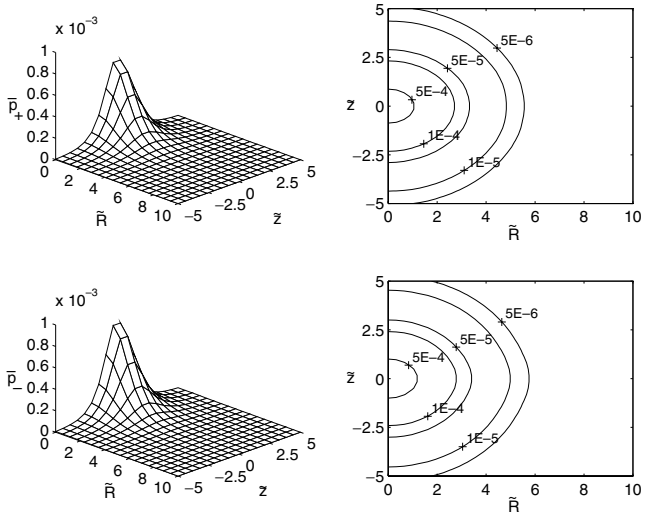

Figure 7. Surface plot and level curves of the pressures $\bar{p}_{\pm}$ equation (26) with parameters $\tilde{a} = 1$ and $\tilde{b} = 2$.

The surfaces and level curves of the densities equations (29) and (30) and pressures equation (26) are shown in Figs 6 and 7, respectively, for parameters $\tilde{a} = 1$ and $\tilde{b} = 2$. Fig. 8(a) displays the surface and level curves for the azimuthal pressure. For these parameters we have $\tilde{p}_{\varphi}/\tilde{\sigma} < 0.3$, $\tilde{p}_{+}/\tilde{\sigma} < 0.25$ and $\tilde{p}_{-}/\tilde{\sigma} < 0.3$.

The tangential circular velocity equation (11) and specific angular momentum equation (12) are given by

$$\left(\frac{v_c}{c}\right)^2 = \frac{2\tilde{R}^2\chi^{3/2}\left[\tilde{R}^2 + \eta(4\tilde{a} + \tilde{b})\right]}{\left[\chi^{3/2} - \tilde{R}^2 - \eta(2\tilde{a} + \tilde{b})\right]\left[\chi^{5/2} - \tilde{R}^4 - 5\tilde{a}\eta\tilde{R}^2 + \eta^3(2\tilde{a} + \tilde{b})\right]}, \tag{36}$$

$$\bar{h} = \frac{\sqrt{2}\tilde{R}^2\left[\chi^{3/2} + \tilde{R}^2 + \eta(2\tilde{a} + \tilde{b})\right]^2\sqrt{\tilde{R}^2 + \eta(4\tilde{a} + \tilde{b})}}{\chi^{9/4}}\left\{\chi^4 + \left[\tilde{R}^2 + \eta(2\tilde{a} + \tilde{b})\right]\left[\tilde{R}^4 + 5\tilde{a}\eta\tilde{R}^2 - \eta^3(2\tilde{a} + \tilde{b})\right]\right.$$
$$\left. - 4\tilde{R}^2\chi^{3/2}\left[\tilde{R}^2 + \eta(4\tilde{a} + \tilde{b})\right]\right\}^{-1/2}, \tag{37}$$

where $h = cr_s\bar{h}$, $\eta = \tilde{a} + \tilde{b}$ and $\chi = \tilde{R}^2 + \eta^2$. The first-order expansion of equation (36) reads

$$\frac{v_c}{c} = \frac{\sqrt{2}\tilde{R}\left[\tilde{R}^2 + (\tilde{a} + \tilde{b})(4\tilde{a} + \tilde{b})\right]^{1/2}}{\left[\tilde{R}^2 + (\tilde{a} + \tilde{b})^2\right]^{5/4}}\left\{1 + \frac{\tilde{R}^2\left[\tilde{R}^2 + (\tilde{a} + \tilde{b})(4\tilde{a} + \tilde{b})\right]}{\left[\tilde{R}^2 + (\tilde{a} + \tilde{b})^2\right]^{5/2}}\right\}. \tag{38}$$

In Figs 9(a) and (b) we display the rotation profiles and curves of specific angular momentum for parameters $\tilde{a} = 1$, $\tilde{b} = 3$ and $\tilde{b} = 2$. As in the previous case, relativistic effects increase the tangential velocity. We also note that the orbits for $\tilde{b} = 3$ and $\tilde{b} = 2$ are all stable.

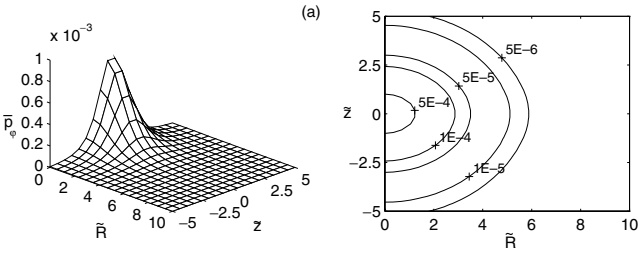

Figure 8. Surface plot and level curves of the azimuthal pressure $\bar{p}_\varphi$ equation (31) with parameters $\tilde{a} = 1$ and $\tilde{b} = 2$.

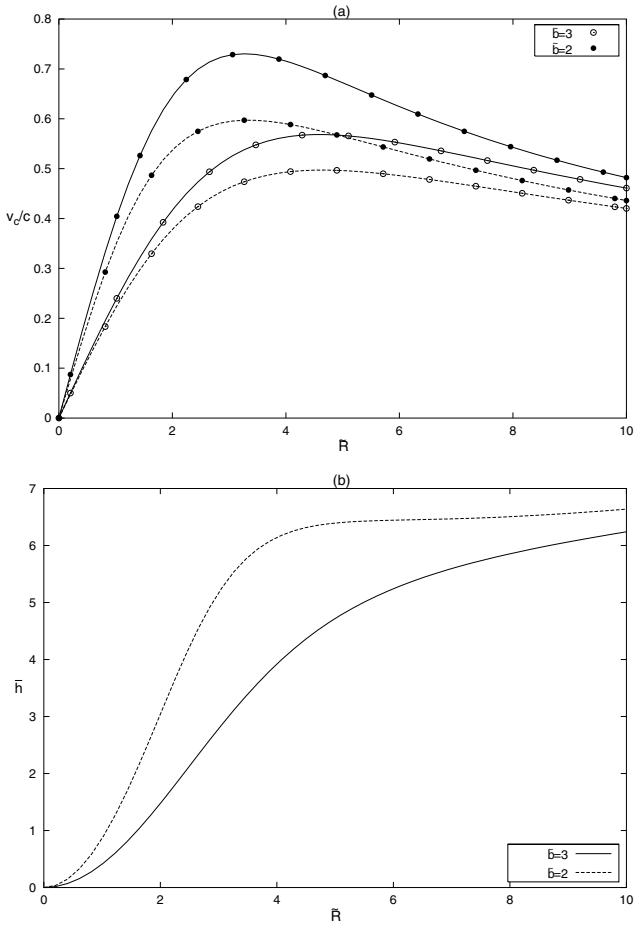

Figure 9. (a) Relativistic rotation profile equation (36) and Newtonian rotation profile (dashed curves) with parameters $\tilde{a} = 1$, $\tilde{b} = 3$ and $\tilde{b} = 2$. (b) Specific angular momentum equation (37) for the same parameters.

4 A GENERAL RELATIVISTIC SATOH MODEL

Satoh (1980) derived other pairs of three-dimensional potential and density functions by inflating the Plummer models of order n. In the limit when $n \to \infty$ the pair takes the simple form

$$\Phi(R, z) = -\frac{Gm}{\sqrt{R^2 + z^2 + a(a + 2\sqrt{z^2 + b^2})}}, \tag{39a}$$

$$\rho_N(R, z) = \frac{ab^2 M}{4\pi} \frac{\left[R^2 + z^2 + (a + 2\sqrt{z^2 + b^2})(a + 3\sqrt{z^2 + b^2})\right]}{(z^2 + b^2)^{3/2} \left[R^2 + z^2 + a(a + 2\sqrt{z^2 + b^2})\right]^{5/2}}. \tag{39b}$$

Using the function $f(R, z)$ with Φ given by equation (39a), we obtain the following expressions for the non-zero components of the energy-momentum tensor equations (4a)–(4e)

$$\bar{\sigma} = \frac{\tilde{a}\tilde{b}^2\left[\tilde{R}^2+\tilde{z}^2+(\tilde{a}+2\xi)(\tilde{a}+3\xi)\right]}{8\pi\xi^3\left[1+\sqrt{\tilde{R}^2+\tilde{z}^2+\tilde{a}(\tilde{a}+2\xi)}\right]^5}, \tag{40a}$$

$$\bar{p}_R = \bar{p}_\varphi = \frac{\tilde{a}\tilde{b}^2\left[\tilde{R}^2+\tilde{z}^2+(\tilde{a}+2\xi)^2\right]}{8\pi\xi^3\left[1+\sqrt{\tilde{R}^2+\tilde{z}^2+\tilde{a}(\tilde{a}+2\xi)}\right]^5\left[-1+\sqrt{\tilde{R}^2+\tilde{z}^2+\tilde{a}(\tilde{a}+2\xi)}\right]}, \tag{40b}$$

$$\bar{p}_z = \frac{\tilde{a}\tilde{b}^2(\tilde{a}+2\xi)}{4\pi\xi^2\left[1+\sqrt{\tilde{R}^2+\tilde{z}^2+\tilde{a}(\tilde{a}+2\xi)}\right]^5\left[-1+\sqrt{\tilde{R}^2+\tilde{z}^2+\tilde{a}(\tilde{a}+2\xi)}\right]}, \tag{40c}$$

$$\bar{\rho} = \frac{\tilde{a}\tilde{b}^2\sqrt{\tilde{R}^2+\tilde{z}^2+\tilde{a}(\tilde{a}+2\xi)}\left[\tilde{R}^2+\tilde{z}^2+(\tilde{a}+2\xi)(\tilde{a}+3\xi)\right]}{4\pi\xi^3\left[1+\sqrt{\tilde{R}^2+\tilde{z}^2+\tilde{a}(\tilde{a}+2\xi)}\right]^5\left[-1+\sqrt{\tilde{R}^2+\tilde{z}^2+\tilde{a}(\tilde{a}+2\xi)}\right]}, \tag{40d}$$

where $\xi = \sqrt{\tilde{z}^2+\tilde{b}^2}$ and the dimensionless variables were previously defined. As f has the form of equation (7), the energy-momentum tensor is diagonal and the radial and azimuthal stresses are equal. We have $\bar{\sigma} > 0$ and $\bar{\rho} > 0$ everywhere and pressures without singularities provided $\tilde{a}(\tilde{a}+2\tilde{b}) > 1$. In the weak field limit, equation (40d) may be expanded as

$$\bar{\rho} \approx \frac{\tilde{a}\tilde{b}^2}{4\pi}\frac{\left[\tilde{R}^2+\tilde{z}^2+(\tilde{a}+2\xi)(\tilde{a}+3\xi)\right]}{\xi^3\left[\tilde{R}^2+\tilde{z}^2+\tilde{a}(\tilde{a}+2\xi)\right]^{5/2}}\left[1-\frac{4}{\sqrt{\tilde{R}^2+\tilde{z}^2+\tilde{a}(\tilde{a}+2\xi)}}\right], \tag{41}$$

which introduces again a negative first-order relativistic correction to the Newtonian mass density.

Expressions for the tangential velocity and angular momentum follow directly from equations (11) and (12)

$$\left(\frac{v_c}{c}\right)^2 = \frac{2\tilde{R}^2\sqrt{\tilde{R}^2+\eta}}{\left[-\tilde{R}^2+\eta+(\tilde{R}^2+\eta)^{3/2}\right]\left(-1+\sqrt{\tilde{R}^2+\eta}\right)}, \tag{42}$$

$$\bar{h} = \frac{\sqrt{2}\tilde{R}^2(1+\sqrt{\tilde{R}^2+\eta})^2}{(\tilde{R}^2+\eta)^{3/4}\sqrt{(\tilde{R}^2+\eta)^2+\tilde{R}^2-\eta-4\tilde{R}^2\sqrt{\tilde{R}^2+\eta}}}, \tag{43}$$

where $h = cr_s\bar{h}$ and $\eta = \tilde{a}(\tilde{a}+2\tilde{b})$. The first-order expansion of equation (42) is given by

$$\frac{v_c}{c} = \frac{\tilde{R}\sqrt{2}}{\left[\tilde{R}^2+\tilde{a}(\tilde{a}+2\tilde{b})\right]^{3/4}}\left\{1+\frac{\tilde{R}^2}{\left[\tilde{R}^2+\tilde{a}(\tilde{a}+2\tilde{b})\right]^{3/2}}\right\}. \tag{44}$$

The surfaces and level curves of the densities and pressures equations (40a)–(40d) for parameters $\tilde{a} = 1$ and $\tilde{b} = 2$ are plotted in Figs 10 and 11. We have $\bar{p}_R/\bar{\sigma} < 0.6$ and $\bar{p}_z/\bar{\sigma} < 0.5$, so all energy conditions are satisfied. Rotation profiles and curves of specific angular momentum are displayed in Fig. 12 for parameters $\tilde{a} = 1$, $\tilde{b} = 2$ and $\tilde{b} = 1$. We note that circular orbits are stable for $\tilde{b} = 2$.

5 GEODESIC ORBITS

An interesting application of the general relativistic galactic models is the study of geodesic orbits outside the galactic plane. As an example we calculate numerically two orbits for the first Miyamoto–Nagai model (Section 3.1) and compare them with the Newtonian case.

We solve numerically the geodesic equations of motion

$$\ddot{x}^\mu + \Gamma^\mu_{\alpha\beta}\dot{x}^\alpha\dot{x}^\beta = 0, \tag{45}$$

for metric equation (2), where $\Gamma^\mu_{\alpha\beta}$ are the Christoffel symbols and the dot denote differentiation with respect to the proper time. With the orthonormal tetrad defined as

$$\begin{aligned} e^i_{(t)} &= \tfrac{1+f}{1-f}(1,0,0,0), \qquad e^i_{(R)} = \tfrac{1}{(1+f)^2}(0,1,0,0), \\ e^i_{(z)} &= \tfrac{1}{(1+f)^2}(0,0,1,0), \qquad e^i_{(\varphi)} = \tfrac{1}{R(1+f)^2}(0,0,0,1), \end{aligned} \tag{46}$$

the tetrad components of the four-velocity v^i read

$$v^i = \gamma(1, v\sin\psi\cos\theta, v\sin\psi\sin\theta, v\cos\psi), \tag{47}$$

with $\gamma = 1/\sqrt{1-v^2}$ (we have set $c = 1$). The specific energy and angular momentum of the test particle are

$$\mathcal{E} = \gamma\frac{1-f}{1+f}, \tag{48}$$

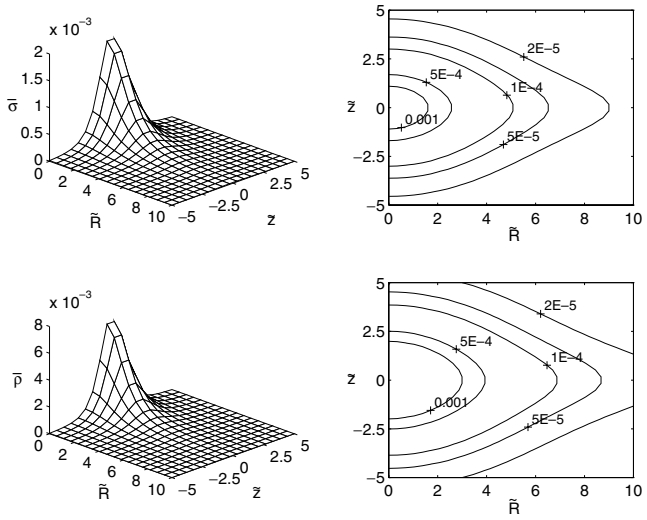

Figure 10. Surface plot and level curves of the energy density $\bar{\sigma}$ equation (40a) and 'effective Newtonian density' $\bar{\rho}$ equation (40d) with parameters $\tilde{a} = 1$ and $\tilde{b} = 2$.

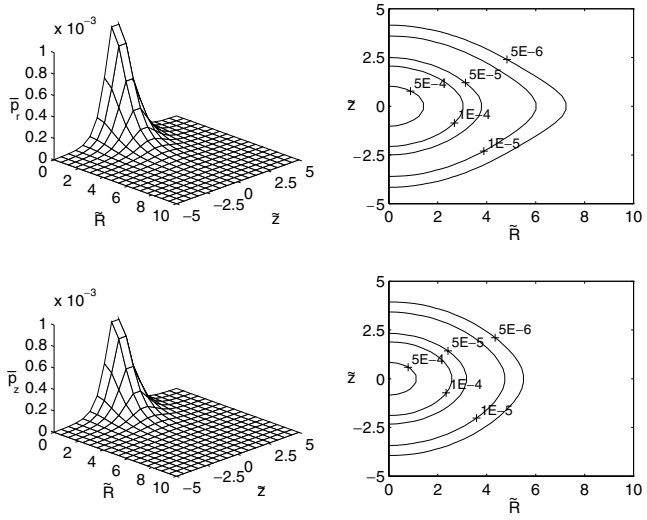

Figure 11. Surface plot and level curves of the radial pressure $\bar{p}_R$ equation (40b) and vertical pressure $\bar{p}_z$ equation (40c) with parameters $\tilde{a} = 1$ and $\tilde{b} = 2$.

$$h = r(1 + f)^2 \gamma v \cos\psi. \tag{49}$$

As initial conditions, we take a position at radius R_0 on the disc's plane and components of the four-velocity $v^i{}_0 = \gamma(1, 0, v_0 \sin\psi, v_0 \cos\psi)$, where v_0 is equal to the tangential velocity of circular orbits at radius R_0. Similar initial conditions for the Newtonian case are chosen with the same angular momentum and energy $\mathcal{E} - 1$. Both the geodesic and Newtonian equations are solved with the fourth–fifth Runge–Kutta method with adaptive size step.

In Figs 13–16 we compare both orbits for the first Miyamoto–Nagai model with parameters $\tilde{a} = 1$ and $\tilde{b} = 1$. For the orbits shown in Figs 13 and 14 large radii have been chosen as initial conditions. As expected, general relativistic effects are small. A noticeable difference is seen in a periodic variation of the amplitude of the $\tilde{R}$ coordinate as a function of the azimuthal angle in the relativistic case. On the other hand, the orbits shown in Figs 15 and 16 have been computed near the centre where the gravitational fields are strong, and the deviation between relativistic and Newtonian orbits are much more pronounced.

6 FIRST-ORDER EFFECTS OF GALACTIC ROTATION ON THE ROTATION PROFILES

The galactic models presented in the previous sections are all static. Astrophysical objects are expected to have angular momentum; thus, more realistic models should incorporate rotation. An exact stationary general relativistic galactic model could be constructed, for example, if one managed to find a closed form of the Kerr metric in terms of elementary functions in stationary isotropic coordinates, and then repeated

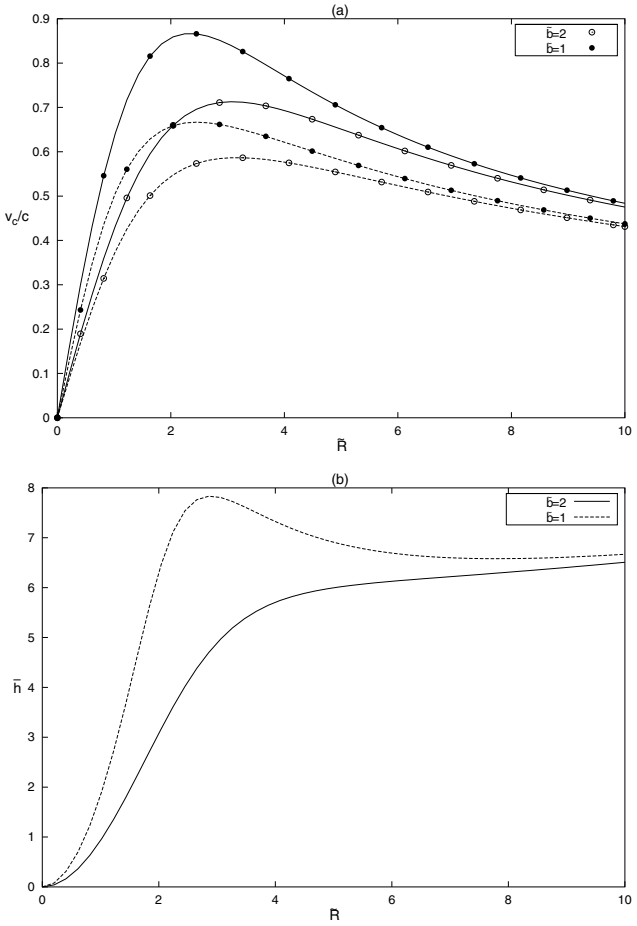

Figure 12. (a) Relativistic rotation profile equation (42) and Newtonian rotation profile (dashed curves) with parameters $\tilde{a} = 1$, $\tilde{b} = 2$ and $\tilde{b} = 1$. (b) Specific angular momentum equation (43) for the same parameters.

the procedure outlined in the previous sections to calculate the matter properties. Although this cannot be done for the exact Kerr solution, the same is not true for the first-order expansion of the Kerr metric with respect to the rotation parameter. It reads

$$\mathrm{d}s^2 = \left(1 - \frac{2GM}{rc^2}\right) c^2\mathrm{d}t^2 - \frac{\mathrm{d}r^2}{1 - (2GM/rc^2)} - r^2(\mathrm{d}\theta^2 + \sin^2\theta\mathrm{d}\varphi^2) + \frac{4GM\alpha}{rc}\sin^2\theta\mathrm{d}t\mathrm{d}\varphi, \tag{50}$$

where α is the rotation parameter. If we transform metric equation (50) to cylindrical isotropic coordinates (t, R, z, φ) and express it in terms of the function f given by equation (3) we obtain

$$\mathrm{d}s^2 = \left(\frac{1-f}{1+f}\right)^2 c^2\mathrm{d}t^2 - (1+f)^4\left(\mathrm{d}R^2 + \mathrm{d}z^2 + R^2\mathrm{d}\varphi^2\right) + \frac{32\alpha R^2 f^3 c^5}{G^2M^2(1+f)^2}\mathrm{d}t\mathrm{d}\varphi. \tag{51}$$

Now the function f may be replaced by any of the forms presented in the previous sections to generate space–times with matter. However, a direct calculation using the Einstein field equations and metric equation (51) shows that the influence of rotation on the physical variables of the matter is of at least $\mathcal{O}(\alpha^2)$. Thus, to have a consistent correction one should also start with metric form equation (51) corrected at least to $\mathcal{O}(\alpha^2)$; however, it does not seem possible to express this particular form of the metric with second-order corrections of the rotation parameter. Despite this, a consistent first-order correction of the rotation profiles can be calculated.

We rewrite equation (51) as

$$\mathrm{d}\tau^2 = g_{tt}\mathrm{d}t^2 - g_{RR}\left(\mathrm{d}R^2 + \mathrm{d}z^2 + R^2\mathrm{d}\varphi^2\right) + 2g_{t\varphi}\mathrm{d}t\mathrm{d}\varphi, \tag{52}$$

where for convenience we have set $c = 1$. Let $v^a = (\dot{t}, 0, 0, \dot{\varphi})$ be the velocity four-vector, where dots denote differentiation with respect to τ. The geodesic equation for circular orbits is

$$g_{tt,R}\dot{t}^2 + 2g_{t\varphi,R}\dot{t}\dot{\varphi} - (R^2 g_{RR})_{,R}\dot{\varphi}^2 = 0 \Rightarrow \frac{\dot{\varphi}}{\dot{t}} = \frac{g_{t\varphi,R} \pm \sqrt{(g_{t\varphi,R})^2 + g_{tt,R}(R^2 g_{RR})_{,R}}}{(R^2 g_{RR})_{,R}}. \tag{53}$$

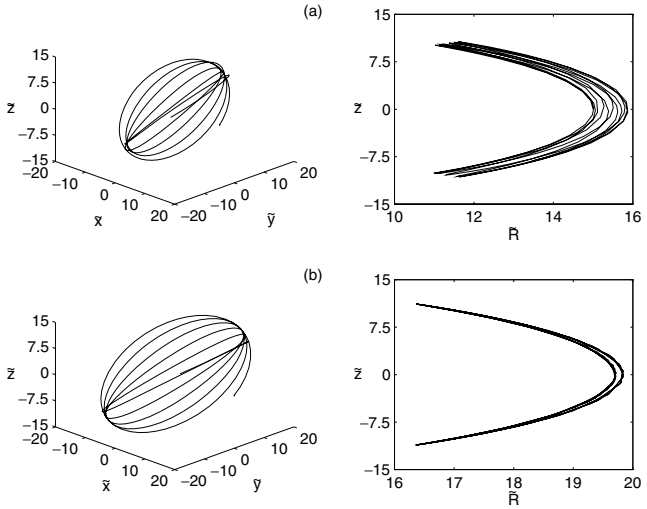

Figure 13. (a) Geodesic orbits for the first Miyamoto–Nagai model with parameters $\tilde{a} = 1, \tilde{b} = 1$. Initial conditions: $\tilde{R}_0 = 15, \psi = 45^\circ$ with energy $\mathcal{E} \approx 0.901$ and angular momentum $\bar{h} \approx 5.03$. (b) Newtonian orbit with energy $\mathcal{E} - 1$ and same angular momentum. Initial conditions: $\tilde{R}_0 \approx 19.84$ and $\psi \approx 36.^\circ 37$.

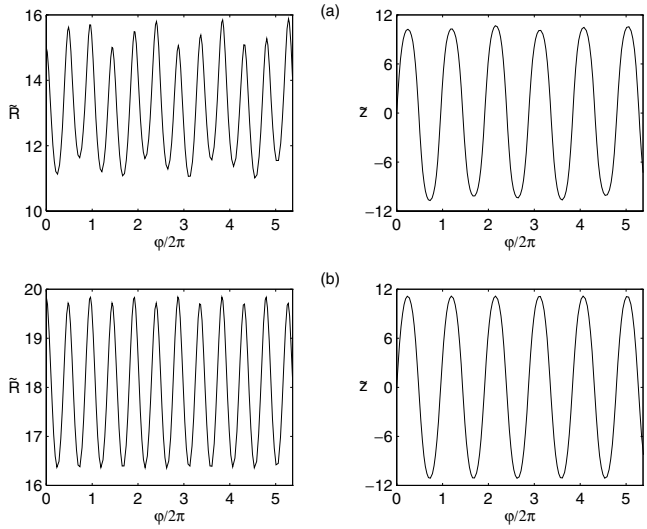

Figure 14. The coordinates $\tilde{R}$ and $\tilde{z}$ as functions of the number of revolutions $\varphi/2\pi$ for the orbits shown in Fig. 13. (a) Geodesic and (b) Newtonian orbit.

Thus, the prograde and retrograde angular velocities are, in general, different. We define an orthonormal tetrad $e_{(b)i}$ as

$$
\begin{aligned}
e_{(t)i} &= \left(\frac{\sqrt{g_{t\varphi}^2 + R^2 g_{tt} g_{RR}}}{R\sqrt{g_{RR}}}, 0, 0, 0 \right), \\
e_{(R)i} &= (0, -\sqrt{g_{RR}}, 0, 0), \quad e_{(z)i} = (0, 0, -\sqrt{g_{RR}}, 0), \\
e_{(\varphi)i} &= \left(\frac{g_{t\varphi}}{R\sqrt{g_{RR}}}, 0, 0, -R\sqrt{g_{RR}} \right),
\end{aligned}
\tag{54}
$$

and project the components of v^a on the tetrad: $\mathbf{v}^{(a)} = e_i^{(a)} v^i = \eta^{(a)(b)} e_{(b)i} v^i$

$$
\mathbf{v}^{(t)} = \frac{\sqrt{g_{t\varphi}^2 + R^2 g_{tt} g_{RR}}}{R\sqrt{g_{RR}}} \dot{t}, \tag{55a}
$$

$$
\mathbf{v}^{(\varphi)} = -\frac{g_{t\varphi}}{R\sqrt{g_{RR}}} \dot{t} + R\sqrt{g_{RR}} \dot{\varphi}. \tag{55b}
$$

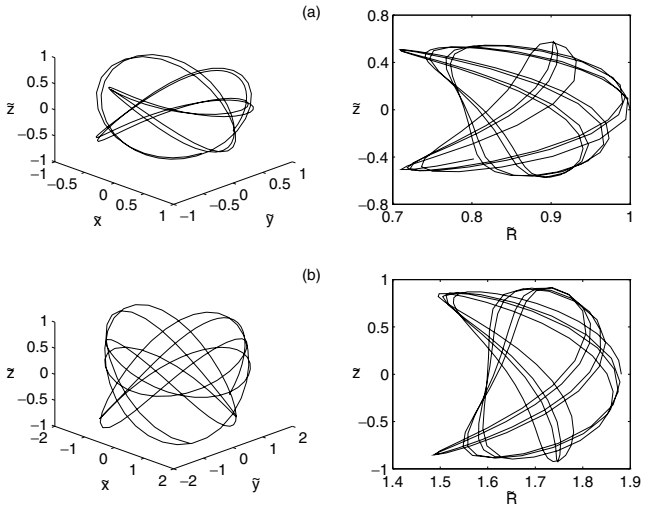

Figure 15. (a) Geodesic orbits for the first Miyamoto–Nagai model with parameters $\tilde{a} = 1$, $\tilde{b} = 1$. Initial conditions: $\tilde{R}_0 = 1$, $\psi = 45^\circ$ with energy $\mathcal{E} \approx 0.196$ and angular momentum $\tilde{h} \approx 0.867$. (b) Newtonian orbit with energy $\mathcal{E} - 1$ and same angular momentum. Initial conditions: $\tilde{R}_0 \approx 1.88$ and $\psi \approx 38.^\circ 01$.

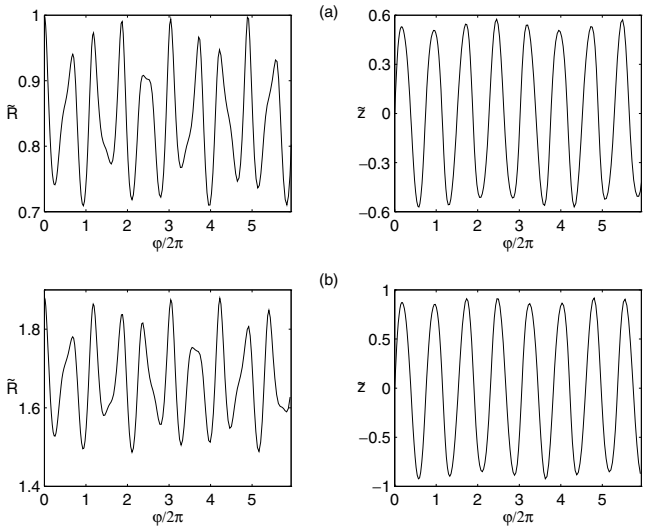

Figure 16. The coordinates $\tilde{R}$ and $\tilde{z}$ as functions of the number of revolutions $\varphi/2\pi$ for the orbits shown in Fig. 15. (a) Geodesic and (b) Newtonian orbit.

Using equation (53) in equations (55a) and (55b) we obtain

$$\frac{\mathbf{v}^{(\varphi)}}{\mathbf{v}^{(t)}} = \frac{1}{\sqrt{g_{t\varphi}^2 + R^2 g_{tt} g_{RR}}} \left[-g_{t\varphi} + \frac{R^2 g_{RR}}{(R^2 g_{RR})_{,R}} \left(g_{t\varphi,R} \pm \sqrt{(g_{t\varphi,R})^2 + g_{tt,R}(R^2 g_{RR})_{,R}} \right) \right]. \tag{56}$$

The terms $g_{t\varphi}^2$ and $(g_{t\varphi,R})^2$ in equation (56) are of $\mathcal{O}(\alpha^2)$ and thus can be neglected. Using metric equation (51), equation (56) can be rearranged as

$$v_c = c\sqrt{\frac{-2Rf_{,R}}{(1-f)(1+f+2Rf_{,R})}} \left[\pm 1 + \frac{24\alpha f^2 R c^4}{G^2 M^2 (1+f)^3} \sqrt{\frac{-Rf_{,R}(1-f)}{2(1+f+2Rf_{,R})}} \right], \tag{57}$$

where c has been reintroduced. The term outside the brackets is the tangential velocity equation (11). The term with α is always positive, and thus the first-order effect of rotation increases (decreases) the prograde (retrograde) tangential velocity.

Equation (57), calculated with the functions f used in Sections 3 and 4, results in

$$\frac{v_c}{c} = \frac{\sqrt{2}\tilde{R}(\tilde{R}^2+\xi)^{1/4}}{[-1+(\tilde{R}^2+\xi)^{1/2}]^{1/2}[-\tilde{R}^2+\xi+(\tilde{R}^2+\xi)^{3/2}]^{1/2}} \left[\pm 1 + \frac{3\tilde{\alpha}\tilde{R}^2(\tilde{R}^2+\xi)^{1/4}}{[1+(\tilde{R}^2+\xi)^{1/2}]^3} \sqrt{\frac{2[-1+(\tilde{R}^2+\xi)^{1/2}]}{-\tilde{R}^2+\xi+(\tilde{R}^2+\xi)^{3/2}}} \right], \tag{58}$$

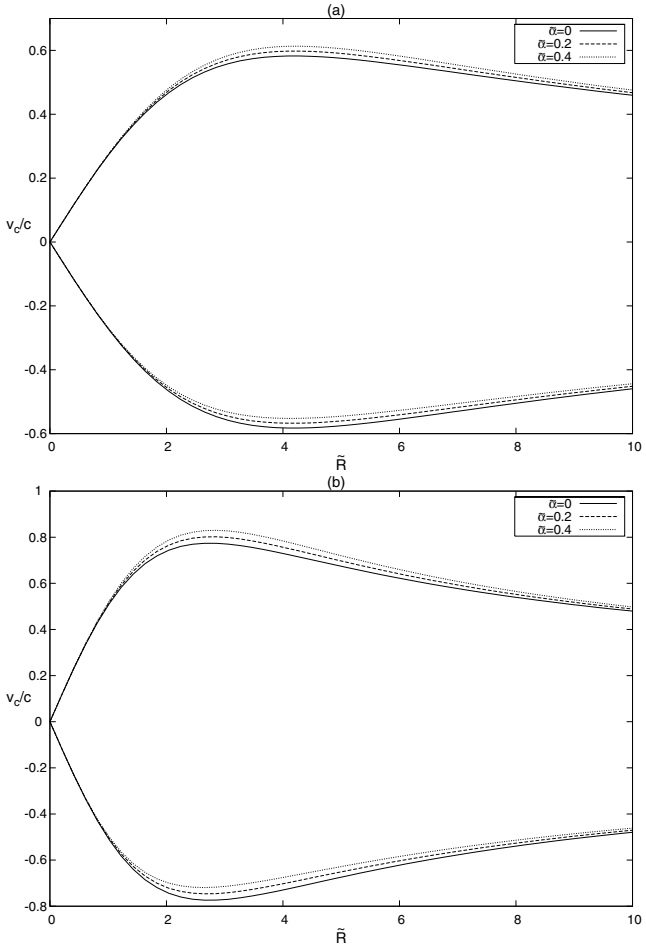

Figure 17. Prograde (upper) curves and retrogade (lower) curves of tangential velocity equation (58) for the first Miyamoto–Nagai model with parameters (a) $\tilde{a} = 1, \tilde{b} = 2$ and (b) $\tilde{a} = 1, \tilde{b} = 1$. Rotation parameter: $\tilde{\alpha} = 0$ (solid line), $\tilde{\alpha} = 0.2$ and $\tilde{\alpha} = 0.4$.

$$\frac{v_c}{c} = \frac{\sqrt{2}\tilde{R}\zeta^{3/4}[\tilde{R}^2 + (\tilde{a}+\tilde{b})(4\tilde{a}+\tilde{b})]^{1/2}}{\left[\zeta^{3/2} - \tilde{R}^2 - (\tilde{a}+\tilde{b})(2\tilde{a}+\tilde{b})\right]^{1/2}\left[\zeta^{5/2} - \tilde{R}^4 - 5\tilde{a}(\tilde{a}+\tilde{b})\tilde{R}^2 + (\tilde{a}+\tilde{b})^3(2\tilde{a}+\tilde{b})\right]^{1/2}}$$
$$\times\left[\pm 1 + \frac{3\tilde{\alpha}\tilde{R}^2\zeta^{3/4}[\tilde{R}^2 + (\tilde{a}+\tilde{b})(2\tilde{a}+\tilde{b})]^2}{[\zeta^{3/2} + \tilde{R}^2 + (\tilde{a}+\tilde{b})(2\tilde{a}+\tilde{b})]^3}\sqrt{\frac{2[\tilde{R}^2 + (\tilde{a}+\tilde{b})(4\tilde{a}+\tilde{b})][\zeta^{3/2} - \tilde{R}^2 - (\tilde{a}+\tilde{b})(2\tilde{a}+\tilde{b})]}{\zeta^{5/2} - \tilde{R}^4 - 5\tilde{a}(\tilde{a}+\tilde{b})\tilde{R}^2 + (\tilde{a}+\tilde{b})^3(2\tilde{a}+\tilde{b})}}\right]. \quad (59)$$

Here, in equation (58) $\xi = (\tilde{a}+\tilde{b})^2$ for the first Miyamoto–Nagai model (Section 3.1), $\xi = \tilde{a}(\tilde{a}+2\tilde{b})$ for the Satoh model (Section 4), and in equation (59) $\zeta = \tilde{R}^2 + (\tilde{a}+\tilde{b})^2$ for the second Miyamoto–Nagai model (Section 3.2). The dimensionless variables were defined in Section 3.1 and $\tilde{\alpha} = \alpha/r_s$.

In Figs 17(a) and (b) we plot the curves of progade and retrogade tangential velocity for the first Miyamoto–Nagai model with parameters $\tilde{a} = 1, \tilde{b} = 2$ and $\tilde{a} = 1, \tilde{b} = 1$ with rotation parameter $\tilde{\alpha} = 0, \tilde{\alpha} = 0.2$ and $\tilde{\alpha} = 0.4$. The same curves for the second Miyamoto–Nagai model and for the Satoh model with parameters $\tilde{a} = 1, \tilde{b} = 2$ are shown in Figs 18(a) and (b).

7 DISCUSSION

Using a special form for the metric in cylindrical isotropic coordinates, we have constructed what may be interpreted as the general relativistic versions of some known Newtonian models for three-dimensional distributions of matter in galaxies, like those formulated by Miyamoto & Nagai (1975), Nagai & Miyamoto (1976) and Satoh (1980). For the first Miyamoto–Nagai potential and for one Satoh potential we obtained matter distributions that have similar properties: their energy-momentum tensor is diagonal with isotropy of pressure in the radial and azimuthal directions; energy density and the 'effective Newtonian density' are positive everywhere as well as the stresses (pressures) in the vertical direction. For particular values of the free parameters, we found that the dominant energy condition is also satisfied. Stability analysis of the circular geodesic orbits on the galactic plane using an extension of the Rayleigh criteria of stability shows stable orbits for some combination

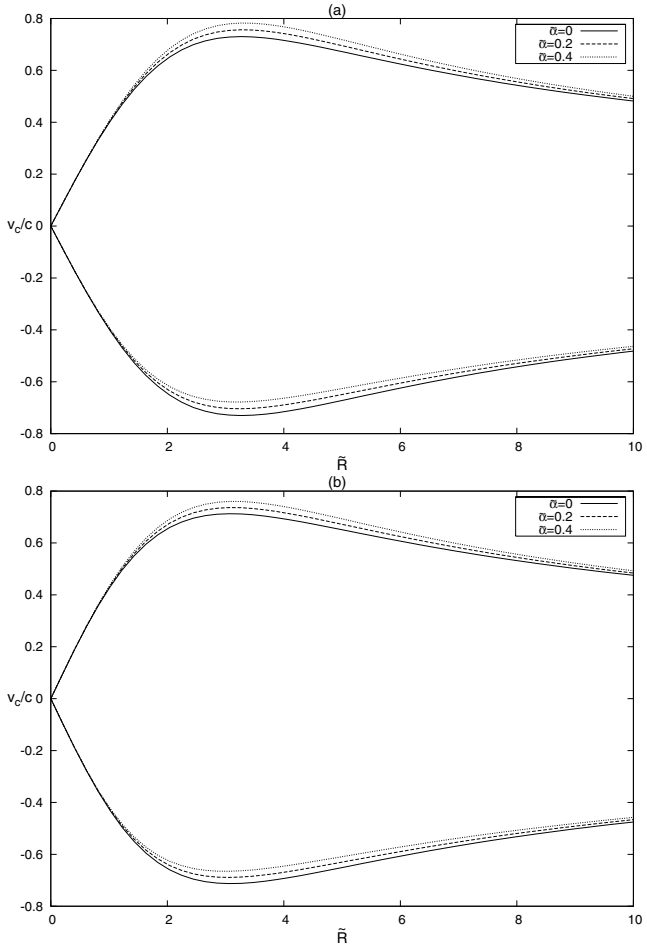

Figure 18. Prograde (upper) curves and retrogade (lower) curves of tangential velocity for (a) the second Miyamoto–Nagai model equation (59) with parameters $\tilde{a} = 1, \tilde{b} = 2$ and (b) for the Satoh model equation (58) with parameters $\tilde{a} = 1, \tilde{b} = 2$. Rotation parameter: $\tilde{\alpha} = 0$ (solid line), $\tilde{\alpha} = 0.2$ and $\tilde{\alpha} = 0.4$.

of free parameters. The second Miyamoto–Nagai potential function, after diagonalization of the energy-momentum tensor, yields matter distributions with positive energy density and three different pressures. Also in this case, free parameters can be chosen so that all energy conditions are satisfied and circular orbits are stable on the galactic plane.

As an example of application of the models, we have numerically calculated some geodesic orbits for one of the potentials and compared them with the Newtonian orbits with the same energy and angular momentum. Near the central regions where the gravitational fields are strong, the motion of particles is considerably altered by general relativistic effects.

We also calculated the first-order effects of galactic rotation on the tangential velocity of circular orbits on the galactic plane using an approximate form of the Kerr metric expressed in cylindrical isotropic coordinates. In general, rotation increases the progade tangential velocity and has an opposite effect on the retrogade tangential velocity.

It should be mentioned that the stability study of the models presented based on the extension of Rayleigh criteria of stability is very limited. A more realistic stability analysis should rely on the first-order perturbed general relativistic fluid equations taking into account two spatial coordinates, which may be not a trivial task (see, for instance, Ujevic & Letelier 2004 for the one-dimensional case). This will be the subject of further investigation.

ACKNOWLEDGMENTS

DV thanks CAPES for financial support. PSL thanks CNPq and FAPESP for financial support. This research has made use of NASA's Astrophysics Data System.

REFERENCES

Bičák J., Ledvinka T., 1993, Phys. Rev. Lett., 71, 1669
Bičák J., Lynden-Bell D., Katz J., 1993a, Phys. Rev. D, 47, 4334
Bičák J., Lynden-Bell D., Pichon C., 1993b, MNRAS, 265, 126

Binney S., Tremaine S., 1987, Galactic Dynamics. Princeton Univ. Press, Princeton, NJ
Bonnor W. A., Sackfield A., 1968, Commun. Math. Phys., 8, 338
Frauendiener J., Klein C., 2001, Phys. Rev. D, 63, 084025
García G., González G., 2004, Phys. Rev. D, 69, 124002
González G., Espitia O. A., 2003, Phys. Rev. D, 68, 104028
González G., Letelier P. S., 1999, Class. Quantum Grav., 16, 479
González G., Letelier P. S., 2000, Phys. Rev. D, 62, 064025
González G., Letelier P. S., 2004, Phys. Rev. D, 69, 044013
Karas V., Huré J. M., Semerák O., 2004, Class. Quantum Grav., 21, R1
Katz J., Bičák J., Lynden-Bell D., 1999, Class. Quantum Grav., 16, 4023
King I. R., 1966, AJ, 71, 64
Klein C., 1997, Class. Quantum Grav., 14, 2267
Klein C., 2001, Phys. Rev. D, 63, 064033
Klein C., 2002, Phys. Rev. D, 65, 084029
Klein C., 2003a, Phys. Rev. D, 68, 027501
Klein C., 2003b, Ann. Phys., 12(10), 599
Klein C., Richter O., 1999, Phys. Rev. Lett., 83, 2884
Kuzmin G. G., 1956, AZh, 33, 27
Landau L. D., Lifshitz E. M., 1987, Fluid Mechanics, 2nd edn. Pergamon Press, Oxford
Lemos J. P. S., 1989, Class. Quantum Grav., 6, 1219
Lemos J. P. S., Letelier P. S., 1993, Class. Quantum Grav., 10, L75
Lemos J. P. S., Letelier P. S., 1994, Phys. Rev. D, 49, 5135
Lemos J. P. S., Letelier P. S., 1996, Int. J. Mod. Phys. D, 5, 53
Letelier P. S., 1999, Phys. Rev. D, 60, 104042
Letelier P. S., 2003, Phys. Rev. D, 68, 104002
Letelier P. S., Oliveira S. R., 1987, J. Math. Phys., 28, 165
Lynden-Bell D., Pineault S., 1978, MNRAS, 185, 679
Miyamoto M., Nagai R., 1975, PASJ, 27, 533
Morgan T., Morgan L., 1969, Phys. Rev., 183, 1097
Morgan L., Morgan T., 1970, Phys. Rev. D, 2, 2756
Nagai R., Miyamoto M., 1976, PASJ, 28, 1
Neugebauer G., Meinel R., 1995, Phys. Rev. Lett., 75, 3046
Plummer H. C., 1911, MNRAS, 71, 460
Rayleigh J. W. S., 1917, Proc. R. Soc. London A, 93, 148
Satoh G., 1980, PASJ, 32, 41
Toomre A., 1963, ApJ, 138, 385
Ujevic M., Letelier P. S., 2004, Phys. Rev. D, 70, 084015
Vogt D., Letelier P. S., 2003, Phys. Rev. D, 68, 084010
Vogt D., Letelier P. S., 2004, Phys. Rev. D, 70, 064003

This paper has been typeset from a TEX/LATEX file prepared by the author.